Experimental study of granular flows in a rough annular shear cell

Venkata Jasti and C. Fred Higgs III*
Mechanical Engineering Department, Carnegie Mellon University, 5000 Forbes Avenue, Pittsburgh, Pennsylvania 15213-3890, USA
(Received 26 February 2008; revised manuscript received 1 June 2008; published 21 October 2008)

The study of granular flows in physics has always been important because of their recurring presence in nature and industry. However, the nonlinear and multiphase behavior exhibited by these particulate systems makes them hard to model and predict. Several experiments were conducted in the past to gain insight into granular flows. The current experimental work furthers this insight and specifically attempts to understand the effect of rough surfaces on granular flows, namely, their local flow behavior. Understanding this interaction can have implications on industrial-scale granular problems. In this work, a granular shear cell, a two-dimensional annular shear cell, was developed to conduct shear experiments where roughness is imposed on the driving surface and experimentally quantified. A digital particle tracking velocimetry data retrieval scheme was developed to extract solid fraction, velocity, and granular temperature data from the experiments as a function of the roughness factor and wheel rotation rate. In general, the steady-state results show the two distinct regions as expected—a high-velocity and dilute-gas-like kinetic region near the moving wall and a high-solid-fraction liquid-like frictional flow regime away from the moving wall. Parametric studies conducted show that the normalized slip near the moving wall decreases with increasing wall roughness and decreasing wall rotation rate. Slip is an important parameter which can be easily interpreted as momentum transfer or traction performance in granular systems related to wheel-terrain interaction, agricultural processing, and most notably granular lubrication.

DOI: 10.1103/PhysRevE.78.041306 PACS number(s): 83.80.Fg, 45.70.−n

I. INTRODUCTION

Understanding granular flows has always been important to predict natural phenomena such as avalanches, landslides, and soil erosion, in addition to industrial processes such as coal transporting and food processing. While granular flows exhibit fluidlike behavior under specific conditions, there are no universally accepted and applicable equations of motion governing their behavior. Fluid motion is governed by the Navier-Stokes equations under all conditions where the fluid is a continuum, but continuum-based granular motion equations govern only specific regimes, such as the kinetic (i.e., gaslike) regime [1], but no equations span all regimes. This is because of the intermittent multiphase behavior and the intrinsic energy dissipation of granular flows. Experiments and models focusing on specific regimes or granular problems such as segregation, heap formation, hopper flow, and silos have been used to gain insight into the behavior of granular flows. While some work has been done to understand them under shear, a detailed experimental investigation to understand their interaction with varying levels of rough surfaces has not been done, and yet can be vital to the understanding of some granular phenomena. The momentum transfer from a rough driving surface to granular particles is of paramount importance in understanding the energy imparted to a granular flow.

Following the detailed work of Bagnold [2], numerous granular shear experiments were conducted. The current setup is similar to annular shear cells where the concentric cylinders move relative to each other, creating a net shear on the granular flow in between. GDR MiDi [3] gives a good account of a collection of such experiments and also identifies some common flow features in their analysis. Tardos *et al.* [4] sheared glass beads between concentric cylinders but the measurements were limited to the global torque and did not include discrete particle measurements of the local flow. However, local measurements were addressed by Veje *et al.* [5] using particle tracking techniques that recorded both particle velocities and spins. Tracking of the local properties was further extended into the third dimension by using a combination of magnetic resonance imaging, x-ray tomography, and digital particle tracking techniques in Mueth *et al.* [6]. One collective difference between the above experiments, other similar setups [7,8], and the current problem is the magnitude of shear rate and the cell rotation rate (in rpm). In the aforementioned shear cells, the relatively moving surfaces had significantly lower rotation speeds than that occurring in the current granular shear flow experiments. This is because the authors have interest in studying granular flows in bearinglike environments, where hydrodynamic fluids are typically sheared at linear speeds on the order of m/s to km/s. However, these ultrarapid granular shear flows still exhibited typical granular behavior, namely, the formation of shear bands, rapid velocity changes in the radial direction, and the existence of distinct kinetic and frictional flow regimes. The experiments performed by Elliot *et al.* [9] were at high speeds similar to the current work, but their shear cells had both the inner and the outer boundaries moving in opposite and relative motion, which enabled the entire flow to be maintained in the kinetic region. In tribology (see the exhaustive review by Wornyoh *et al.* [10]), the grain inertia or kinetic regime leads to what is called "granular kinetic lubrication," where parallel surfaces can be separated due to granular collisions. The frictional or macroviscous regime is referred to as "granular contact lubrication" in sliding con-

*FAX: (412)-468-3348. higgs@andrew.cmu.edu

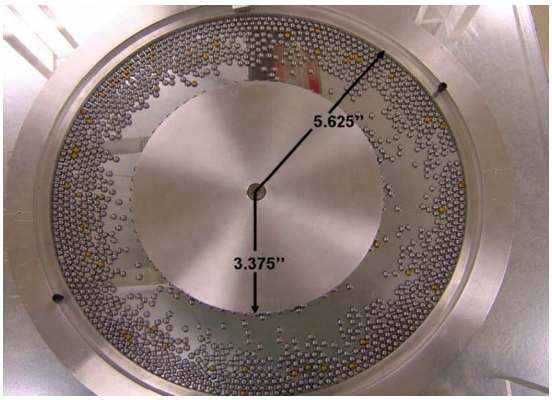

FIG. 1. (Color online) Top view of the granular shear cell (GSC). Gravity acts into the page.

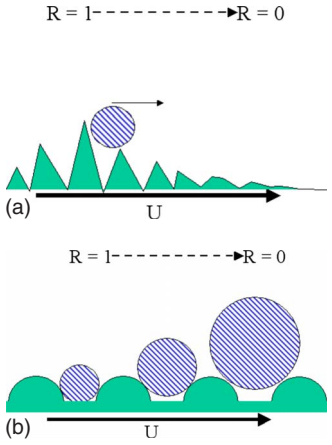

FIG. 2. (Color online) Roughness factors R defined as (a) the fraction of lateral momentum imparted by the surface and (b) the fraction of granules that fits between wall particles

tacts, where the granules are in enduring contact and move in layers relative to adjacent layers.

Most of the above experiments realized the importance of having macroscopic roughness on the boundary. Consequently, the authors glued particles [6,7] or toothed belts [9] to the driving wheel to achieve an effective roughness factor. Their macroscopic roughness was random, unquantified, or deterministically fixed. Understanding the effect of this macroscopic roughness on the granular shear is very important when studying and precisely controlling granule-surface interactions. Therefore, the current work focuses on the granular flow behavior in an annular shear cell, where one surface with a prescribed roughness factor drives the flow. Since only one of the two annular surfaces is moving, both the kinetic and frictional regimes exist in the granular shear cell. Within this cell, the local flow properties—velocity, solid fraction, granular temperature and slip—of the granular flow are measured as functions of the roughness factor and wheel rotation rate.

II. EXPERIMENTAL SETUP

A. Shear cell description

An annular shear cell was fabricated to study the behavior of granular flows in a shear cell, where the rotating wheel has a prescribed roughness. The top view of the granular shear cell (GSC) is shown in Fig. 1, where the direction of gravity is into the page. It has an aluminum frame with a transparent Plexiglas body so that the dynamic behavior of the granular flow can be observed. Additionally, the bottom surface that the granules roll on is smooth Plexiglas with an estimated low rolling friction coefficient of $\mu_R < 0.15$ (i.e., μ_R decreases with increased speed [11]). The top surface is also Plexiglas which confines the granules into a two-dimensional $(r\text{-}\theta)$ plane by preventing them from jumping into the third dimension (out of the page). The moving wheel is attached to a 1/16 hp motor capable of achieving a constant rotational speed of approximately 53–280 rpm, which corresponds to a linear velocity of 0.55–2.89 m/s. The wheel radius is 8.5725 cm (3.375 in.) and the distance from the center of the wheel to the stationary outer rim is 14.2875 cm (5.625 in.). Thus, the gap, which is the distance between the moving wheel and outer rim, is approximately 5.71 cm (2.25 in.). The granules are made of milled shock-resistant water-hardened S2 tool steel (from McMaster-Carr, part no. 1995T11) with Rockwell C55–C58 hardness and 290 000 psi yield strength. The diameter of the spherical granules is 0.476 25 cm (3/16 in.). The shear gap is filled with an area solid fraction of 0.708, which means that approximately 70% of the overall gap area is filled with the granules during operation. While the GSC was built for a monolayer of granules, the spacing between the bottom and top Plexiglas surfaces was set to 0.762 cm (0.3 in.), which is slightly larger than a granule diameter, to allow the particles to freely move in the gap without being constrained by the friction from both the top and bottom GSC Plexiglas surfaces. The total number of granules put into the GSC is 1633.

B. Wheel roughness

As defined by the authors, the roughness factor R varies as $0 \leqslant R \leqslant 1$, where $R=0$ corresponds to a moderately smooth surface, and $R=1$ to a very rough surface. Figure 2 shows that the literature has interpreted the roughness factor R as (1) the fraction of lateral momentum transferred to the granular flow by the walls [12] and (2) the fraction of granules that fit exactly between the cylindrical wall disks [13]. The authors chose to define the roughness factor R similarly to Jenkins and Richman's description (2) above, which is the fraction of granules that fits between the wall hemispheres, but not exactly the same. For example, $R=0$ in this experimental work means that the hemispheres are directly adjacent to each other with no spacing for a granule to fit between them, while $R=1$ means that the gap between adjacent hemispheres is one granule diameter d. This is different from Jenkins and Richman's theoretical roughness factor R' which is defined as the ratio $(d+s)/(d+\sigma)$, where d and σ are the diameters of the flow granules and wall granules, respectively, and s is the separation between the adjacent wall granules. To avoid substrate effects, they impose a limit on the maximum separation s between two adjacent granules. Thus, a continuum model employing Jenkins and Richman's

TABLE I. Conversion to Jenkins and Richman roughness factor.

R (Experimental roughness factor)	R' (Jenkins and Richman factor)
0	0.5
0.2	0.6
0.4	0.7
0.6	0.8
0.8	N/A
1	N/A

roughness factor R' to model our work should only use the data for $R \leqslant 0.6$ (see Table I). This definition is easy to physically implement in granular experiments in a mathematically quantifiable way, as shown in Fig. 3. The GSC has a set of interchangeable inner wheels, where each has a prescribed roughness in the form of steel hemispheres protruding from the aluminum wheel. The roughness factor can vary from $R=0$ (see bottom wheel in Fig. 3) to $R=1$ (see top wheel in Fig. 3).

C. Data acquisition: Digital particle tracking velocimetry

A digital particle tracking velocimetry (DPTV) data retrieval scheme was developed to track the individual position (x,y) or $(r\text{-}\theta)$ of each particle as a function of time. In this scheme, a digital video camera operating at 3000 frames/s and with a resolution of 512×384 pixels filmed the colliding granules in the GSC during operation [Fig. 4(a)]. A computational code was developed in MATHEMATICA to take the video frames as input while utilizing the MATHEMATICA image processing toolbox to threshold the images [Fig. 4(b)], reducing the particles and nonparticles to white and black, respectively. Subsequently, the code computes each particle's centroid [Fig. 4(c)] and tracks them between consecutive frames to calculate velocity of each granule [Fig. 4(d)].

Other DPTV-type particle tracking techniques have been used in the past to study granular shear [5,6]. Xu *et al.* [14] conducted a theoretical study validated by discrete particle computer experiments on the possible errors that can result from using digital particle tracking techniques. The current work took care to minimize the errors resulting from insufficient frame rate or insufficient sampling by choosing a frame rate of 3000 frames/s and analyzing five trials of 450

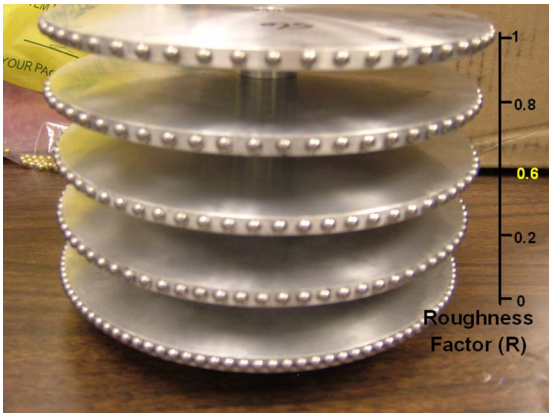

FIG. 3. (Color online) Wheel roughness on GSC: from top to bottom, $R=0$ to 1.

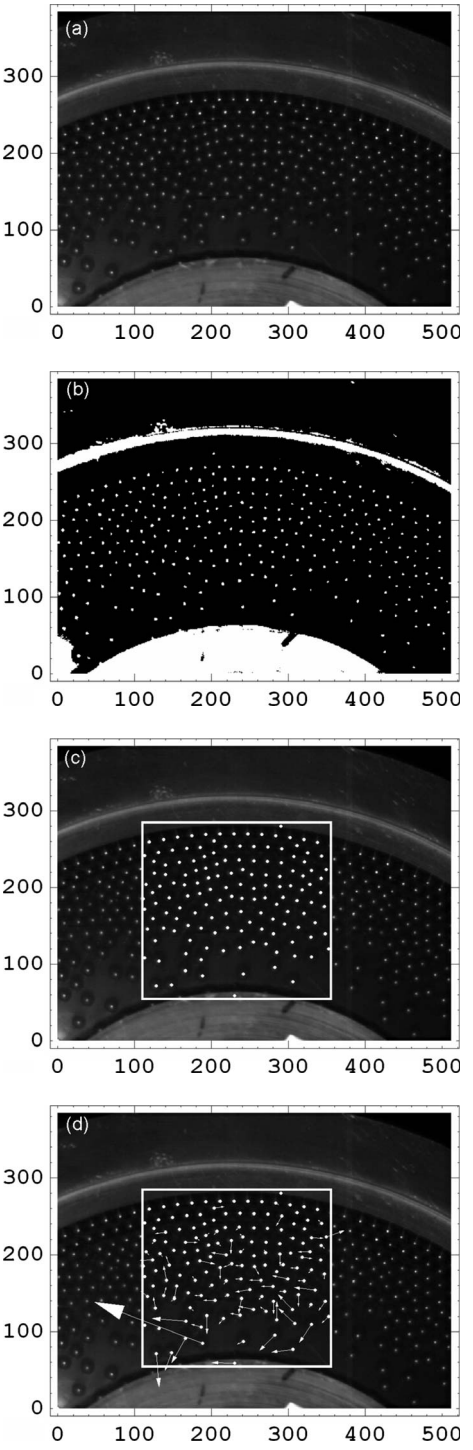

FIG. 4. (a) Image extracted from high-speed video. (b) Thresholding of the image makes granular particles white and nonparticle space black. (c) The DPTV code computes the particle centroids in the area of interest indicated by the white box. (d) The DPTV code also computes the particle velocity vectors that lead to granular flow parameters.

sets of frames for each data point. However, error due to finite pixel size could not be further reduced as the maximum size of the image was limited by the camera capabilities. According to Xu *et al.*, the error in granular temperature due to finite pixel size may be higher in the dense particle region than in the kinetic region, similar to the errors observed in their work. From the position data obtained from particle tracking, granular flow properties such as velocity, solid fraction, granular temperature, and slip can be determined as a function of position and/or time. Additionally, these local flow parameters can be functions of the moving wall roughness, granule size, global solid fraction, and moving wall rotation rate.

III. PROCEDURE AND CALCULATIONS

Two sets of experiments are presented in this work to study the effect of the driving wheel's roughness and rotation rate on the granular flow. For each experiment, a prescribed roughness factor is set by mounting the appropriate inner driving wheel into the granular shear cell. Subsequently, the gap is filled with a fixed number of granules. The granules are randomly arranged inside the GSC gap, which is then closed by placing the Plexiglas on the top before the motor is switched on. Using an infrared tachometer, the rotation rate of the inner wheel is measured and set to the required rpm. The setup is run for 2 min to establish a reasonable steady state before the prescribed area of interest is recorded by the camera. Approximately 3000 frames are then extracted from the video and DPTV is performed by postprocessing 450 sets of consecutive frames selected at equal intervals. Five trials were conducted for each experiment and the averages of the trials are the data points presented in this work.

The experimental results from the GSC are obtained by averaging the discrete kinematic data of individual granules within the prescribed area of interest [see Fig. 5(a)]. The local granular flow properties (e.g., velocity, solid fraction, and granular temperature) were assumed invariant in the tangential direction due to the symmetry of the setup, and vary only in the radial direction. To obtain the local granular flow data as a function of radius, the area of interest was divided into six radial bins and the local flow properties of each bin were calculated from the average kinematic data of the granules in the bin. Each bin has a width of approximately two particle diameters, with respect to the granules used in this work. A normalized bin radius (r_b/r_o) is used for plotting where r_b and r_o are the radii of the bin and outer rim, respectively. It is scaled such that the inner (moving) wheel is at a radius $(r_b/r_o)=0$, and the outer (stationary) rim is at a radius $(r_b/r_o)=1$. For example, Fig. 5(b) shows normalized velocity data as a function of radial position (r_b/r_o). Here, at the radial position $(r_b/r_o)=0.0834$ [which is bin 1 in Fig. 5(a)], the average normalized velocity of the flow in this bin is 0.085.

The following equations were used in calculations:

$$\nu_i = \frac{N_i \pi d^2}{A_i}, \tag{1}$$

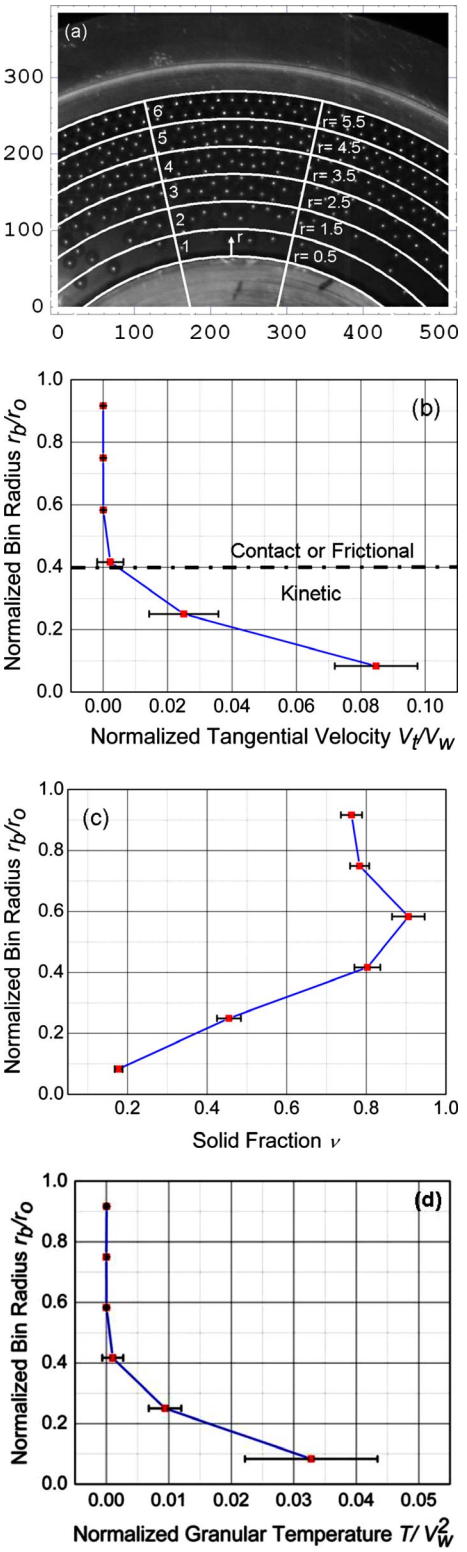

FIG. 5. (Color online) (a) The granular shear cell gap was divided into six radial bins, where bin 1 and bin 6 are adjacent to the inner (moving) and outer (stationary) surfaces, respectively. (b) Normalized radial position vs the normalized tangential velocity. The dotted horizontal line delineates the transition from the granular frictional to the kinetic regime. (c) Normalized radial position vs the local solid fraction. (d) Normalized radial position vs the normalized granular temperature

$$V_{T,i} = \frac{1}{N_i} \sum_{j=1}^{N_i} v_{T,j}, \tag{2}$$

$$T_i = \frac{1}{N_i} \sum_{j=1}^{N_i} \frac{1}{3} [(v_{T,j} - V_{T,i})^2 + (v_{R,j} - V_{R,i})^2], \tag{3}$$

$$S = V_w - V_{T,1}. \tag{4}$$

As shown in Fig. 5(a), the DPTV code was preset to divide the GSC gap into six radial bins. Equation (1) shows that the average solid fraction ν_i in radial bin i can be computed from the number of particles in a bin N_i, the particle diameter d, and the bin area A_i. It is important to note that the solid fraction calculated in this work is area solid fraction and not volume solid fraction. Additionally, hemispherical particles protruding from the wheel take up a fraction of bin 1 which is adjacent to the wheel. Consequently, there is less available room in this bin for the particles to occupy. Equation (2) calculates the average tangential velocity $V_{T,i}$, where $v_{T,j}$ is the tangential velocity of some particle j within a prescribed bin. Equation (3) was used to compute the granular temperature T_i in bin i, where $V_{R,i}$ is the average radial velocity in bin i and $v_{R,j}$ is the radial velocity of some particle j within a prescribed bin i. Equation (4) was used to compute the slip velocity S at the inner moving wheel, where V_w is the linear (i.e., tangential) velocity of the wall and $V_{T,1}$ is the average tangential velocity of bin 1 [see Fig. 5(a)], which is the bin adjacent to the moving wheel.

IV. RESULTS

The plots in Fig. 5 show the quasi steady-state data where each data point is the average of five trials. The horizontal bar through the data points is representative of the experimental data in this paper and indicates one standard deviation. The tangential velocity, slip, and granular temperature data are normalized by some function of the linear wheel velocity V_w. Figure 5(b) shows the change in tangential velocity across the gap for the base case when the GSC was filled with 1633 steel granules with 3/16 in. diameter and the wheel with roughness factor $R=0.6$ was set to 240 rpm. These experimental conditions are applicable throughout this work, unless explicitly stated otherwise. The resulting velocity is highest near the driving wall and rapidly diminishes moving towards the stationary wall. It is worth noting that the centrifugal force, inherent in an annular shear cell configuration, promotes two-phase granular flow behavior as shown in Fig. 5(b). The dotted horizontal line delineates the transition [10,15] from the "granular frictional" [16] regime to the "granular kinetic" [1,17,18] regime. The frictional regime consists of densely packed granules undergoing relative sliding and/or rolling contact in a quasistatic or quasidynamic state, while the kinetic regime is characterized by predominantly collision-based momentum transfer in a fully dynamic state. Figure 5(c) shows variation in local solid fraction across the gap. The solid fraction is lowest near the driving wheel as it expels the granules coming in contact with it. Aided by centrifugal force, most of the granules cluster near the outer stationary wall. It should be noted that the solid fraction exceeds the maximum theoretical packing fraction for circles in the region $0.4<(r_b/r_o)<0.8$. This is because the height [measured out of the page in Fig. 5(a)] between the bottom and top Plexiglas surfaces is slightly greater than the diameter of the granules. Therefore, some granules in the highly packed plug flow region are squeezed together, which causes a partial overlap of particles within the open voids between granules. The radial position versus granular temperature plot is shown in Fig. 5(d). The granular temperature is a measure of the amount of velocity fluctuations in granular flow. The total granular temperature is comprised of the translational granular temperature and the rotational granular temperature, which directly depend on spin. Since the current setup does not measure spin, the translational granular temperature has been plotted. The region adjacent to the moving wall has low solid fraction and high tangential velocities, which promotes binary collisions. This results in higher velocity fluctuations and, hence, the highest granular temperature in the region. The granular temperature also diminishes away from the driving wall, similar to the tangential velocity. It is typical that the granular temperature is low in high-solid-fraction regions due to the loss of particle mobility.

A. Local flow properties as a function of wheel roughness

In this section, the steady-state data for the local granular flow properties of velocity, solid fraction, granular temperature, and slip are presented when our roughness factor R is varied by changing the inner wheels which each have a roughness $R=0$ (smooth) to $R=1$ (rough). Other experimental conditions were maintained constant for this set of experiments.

Figure 6(a) shows the normalized tangential velocity profiles at different roughness factors. As expected, the velocities increase with increasing roughness factor. Additionally, at roughness factors $R=0.8$ and 1, the plug flow region at approximately $0.6<(r_b/r_o)<1$ is diminished compared to when the roughness factor $R<0.8$, where there is a larger plug region spanning approximately $0.4<(r_b/r_o)<1$. Slip near the wheel surface is observed in all the profiles and this will be explored further in Fig. 6(d). Figure 6(b) shows the solid fraction profiles being varied as a function of the roughness factor. It can be observed that an increasing number of granules are packed in the plug flow region as the roughness factor is increased, and the overlapping, as explained earlier in this section, also increases. Interestingly, this overlapping artifact was often observed at the boundary of the contact and kinetic regions. This can be understood in that there will be a major shift in momentum when a particle from the high-energy kinetic region collides with those particles in the low-energy frictional flow region, which causes an impulse force that squeezes some granules into the void spacing between and above the neighboring granules. Figure 6(c) is a plot of the normalized granular temperature profiles as computed by Eq. (3). They exhibit a clear trend of increasing granular temperature with increasing roughness factor and this can be best explained by examining the normalized

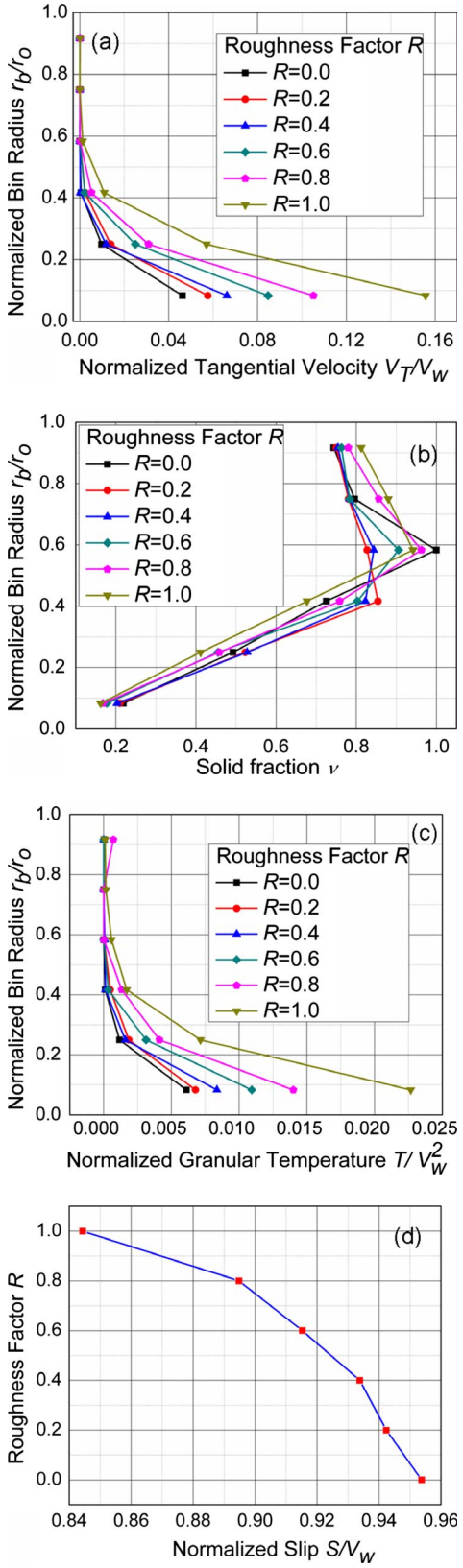

FIG. 6. (Color online) (a) Normalized velocity vs radial location as a function of the roughness factor R. (b) Solid fraction vs radial location as a function of the roughness R. (c) Normalized granular temperature vs radial location as a function of the roughness factor R. (d) Roughness factor vs normalized slip.

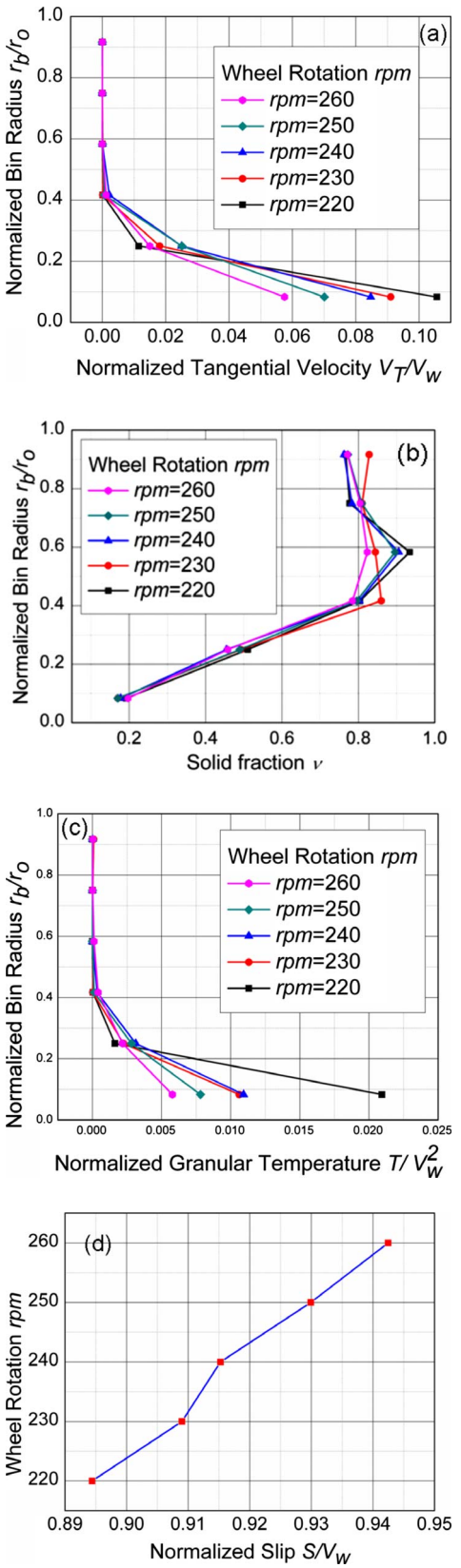

FIG. 7. (Color online) (a) Radial location vs normalized tangential velocity as a function of wheel rotation (rpm). (b) Radial location vs solid fraction as a function of wheel rotation (rpm). (c) Radial location vs normalized granular temperature as a function of wheel rotation (rpm). (d) Wheel rotation vs normalized slip.

velocity and solid fraction in Figs. 6(a) and 6(b). In the region $0<(r_b/r_o)<0.2$ that is adjacent to the moving wheel, the granular velocity rapidly increases with the roughness factor as expected. While the solid fraction in Fig. 6(b) was expected to rapidly decrease with increasing roughness factor R, the actual decrease was steady and less pronounced, thereby yielding less variation in the solid fraction from $R=0$ to 1. This resulted in increased collisions and velocity fluctuations as the roughness factor increases, which led to higher granular temperatures as observed in Fig. 6(c). Figure 6(d) is a plot of the nondimensional slip velocity as computed by Eq. (4), and it is shown as a function of the wheel roughness R. It is consistent with physical intuition and past continuum models [1,19,20] of granular couette shear cells which varied roughness and found slip to be inversely proportional to the roughness factor. One should note that at the roughness factor $R=0$ the normalized slip is not equal to unity. This is because the $R=0$ wheel is only "relatively" smooth; there is still inherent roughness when two spheres (or circles in two dimensions) are put side by side.

B. Local flow properties as a function of wheel rotation speed

In this section, the steady-state data for the local granular flow properties of velocity, solid fraction, granular temperature, and slip are presented when the wheel rotation rate is varied from 220 to 260 rpm. While the setup can achieve rotation rates from 53 to 280 rpm, sustained granular flow is not possible (for the given solid fraction) at lower rotation rates. At these rates, the granules are driven away from the moving wheel and come to rest away from it due to dissipative collisions with each other. The other experimental conditions were maintained constant for this set of experiments.

Figure 7(a) plots the normalized tangential velocity in the gap as a function of wheel rotation rate, and one can see that the kinetic regime still exists for nearly all rotational speeds in the range $0<(r_b/r_o)<0.4$. It is difficult to resolve any trend except at the region nearest to the moving wheel at $(r_b/r_o)=0.1$, where the normalized tangential velocity is inversely proportional to the disk speed. This phenomenon was also observed in a kinetic continuum model [1] for parallel rough shear cells under normal compression. This will be further explained in Fig. 7(d). The solid fraction data [as shown in Fig. 7(b)] do not exhibit a clear trend when the wheel rotation rate is varied. However, they do show that the most dense region occurs at approximately $(r_b/r_o)=0.6$ due to particle overlapping as explained earlier in the results sections, while the most dilute regions occur when $(r_b/r_o)<0.2$ which is nearest the moving wheel. Here, the particles are highly energized and rapidly expelled from wheel contact. The normalized granular temperature in Fig. 7(c) resembles the normalized tangential velocity in Fig. 7(a), except that the fluctuations at a wheel rotation of 230 and 240 rpm are nearly equal. This is possible because the granular temperature accounts for fluctuations in both the radial and tangential directions. Hence, a clear trend in tangential velocity alone cannot ensure a clear trend in granular temperature. The observation in Fig. 7(a) that the normalized granular velocity near the moving wheel is inversely related to the wheel's rotation speed can be explained by the slip, which is plotted in Fig. 7(d) as a function of wheel rotation. For a fixed annular gap, the slip at the wheel increases with wheel rotation speed. It is very important to note that the "normalized" tangential velocity in Fig. 7(a), and not the actual tangential velocity of the granules, is decreasing as the wheel rotation rate increases. Consequently, the ratio of the granular kinetic energy to the wheel kinetic energy decreases, which suggests that the dissipation of the wheel's energy into the granular flow is more efficient at slower wheel speeds. This type of information is useful in granular processing where the optimal particle transport rate is sought.

V. CONCLUSIONS

The motivation of the current work was to understand the interaction of rough surfaces and granular flows. Hence, the granular shear cell, a two-dimensional annular shear cell, was developed to conduct granular shear experiments. A set of interchangeable driving wheels was designed for the setup with different quantifiable roughness factors. The solid fraction, velocity, and granular temperature data were extracted from the experiments using the digital particle tracking velocimetry technique. Experiments were performed for varying values of roughness factor and rotation rate of the driving wheel, and the resulting parametric trends were analyzed. Increase in the roughness factor of the driving wheel resulted in increased tangential velocities, increased granular temperatures, and more granules clustering away from the driving wheel. Additionally, slip at the driving wall decreased significantly as the roughness factor increased. These experimental results numerically quantify the significant effect the boundary roughness factor has on the local flow properties in a couette shear flow. Thus, it is important to have a clearly defined and quantified roughness factor. Parametric studies conducted on the wheel rotation rate show that an increase in the wheel rotation rate resulted in reduced normalized velocities and reduced normalized granular temperatures. While no clear trend was exhibited by the solid fraction data, slip increased with increasing rotation rate. Slip is the key factor that determines the relative amount of wheel momentum that is transferred to the granular flow. It also controls the fraction of the wheel energy being dissipated into the granular flow. This work on boundary interaction related to granular materials can be useful in addressing questions about optimal particle transport rates, in addition to resolving the physics for enabling wheels to traverse granular terrain.

ACKNOWLEDGMENTS

The authors would like to thank the NETL for supporting this work. Additionally, the authors would like to acknowledge the contributions from Joe McCarthy at the University of Pittsburgh and undergraduate researchers in the granular subgroup in the Particle Flow and Tribology Laboratory at Carnegie Mellon. Lastly, the authors appreciate Dr. Kristian Sveen of Cambridge University for his DPIV code for fluids, which was helpful in our developing our own DPTV code for grains.

[1] C. F. Higgs III and J. Tichy, J. Tribol. **126**, 499 (2004).
[2] R. A. Bagnold, Proc. R. Soc. London, Ser. A **225**, 49 (1954).
[3] G. D. R. MiDi, Eur. Phys. J. E **14**, 341 (2004).
[4] G. I. Tardos, M. I. Khan, and D. G. Schaeffer, Phys. Fluids **10**, 335 (1998).
[5] C. T. Veje, D. W. Howell, and R. P. Behringer, Phys. Rev. E **59**, 739 (1999).
[6] D. M. Mueth *et al.*, Nature (London) **406**, 385 (2000).
[7] L. Bocquet, W. Losert, D. Schalk, T. C. Lubensky, and J. P. Gollub, Phys. Rev. E **65**, 011307 (2001).
[8] G. Chambon, J. Schmittbuhl, A. Corfdir, J. P. Vilotte, and S. Roux, Phys. Rev. E **68**, 011304 (2003).
[9] K. E. Elliott, G. Ahmadi, and W. Kvasnak, J. Non-Newtonian Fluid Mech. **74**, 89 (1998).
[10] E. Y. A. Wornyoh, V. K. Jasti, and C. F. Higgs III, J. Tribol. **129**, 438 (2007).
[11] E. Rabinowicz, *Friction and Wear of Materials* (Wiley-Interscience, New York, 1995).
[12] K. Hui *et al.*, J. Fluid Mech. **145**, 223 (1984).
[13] J. Jenkins and M. Richman, J. Fluid Mech. **171**, 53 (1986).
[14] H. Xu, A. P. Reeves, and M. Y. Louge, Rev. Sci. Instrum. **75**, 811 (2004).
[15] C.-M. Yu, K. Craig, and J. Tichy, J. Rheol. **38**, 921 (1994).
[16] L. S. Mohan, K. Kesava Rao, and P. R. Nott, J. Fluid Mech. **457**, 377 (2002).
[17] J. T. Jenkins and C. Zhang, Phys. Fluids **14**, 1228 (2002).
[18] C. K. K. Lun *et al.*, J. Fluid Mech. **140**, 223 (1984).
[19] V. Jasti and C. F. Higgs III, J. Tribol. **128**, 358 (2006).
[20] L. Zhou and M. M. Khonsari, J. Tribol. **122**, 147 (2000).